IEEE Journal of Microwaves

Received 16 September 2020; revised 26 October 2020; accepted 31 October 2020.
Date of current version 7 January 2021.

Digital Object Identifier 10.1109/JMW.2020.3035790

Microwave Imaging in Security—Two Decades of Innovation

SHERIF S. AHMED

(Invited Paper)

Stanford University, Stanford, CA 94305 USA (e-mail: sherifahmed@ieee.org).

ABSTRACT The microwave spectrum is one of the most valuable natural resource used nowadays in communication, navigation, and remote sensing. With over a century of heritage, imaging with electromagnetics had been puzzling researchers and engineers alike. When science and technology advanced enough, early imaging solutions at the lower end of the microwave spectrum were revealed. Airborne synthetic aperture radars (SAR), and later spaceborne SAR, were first to evolve. With their unprecedented capabilities in earth observation and reconnaissance, researchers became even more eager to extend SAR imaging to higher frequencies and for different applications. The last two decades have remarkably delivered breakthroughs and innovations to re-invent microwave technologies for personnel security screening purposes. Microwave signals can safely penetrate clothing and reveal concealed threats, e.g., explosives and firearms, without imposing any health risks or side effects. This paper presents a historical overview of this evolution and highlights the latest advances in security microwave imaging.

INDEX TERMS Microwave imaging, mmWave systems, personnel screening, synthetic aperture radar.

I. INTRODUCTION

Microwave technologies have ever been a keystone in advancing the capabilities of mankind in the domains of communication, navigation, and remote sensing. In the last two decades, microwave technologies have been utilized for security applications as well. Since the Second World War, radar systems were essential for detection at far distances. The high speed of signal propagation and the immunity against weather conditions, both made microwaves the ultimate choice for defense applications. Not longer after the 9/11 tragedy, the development on imaging radar technology has accelerated to provide novel capabilities for strengthening the security measures at airport checkpoints. In such, the microwave signals can easily penetrate clothing and reveal concealed items, e.g., explosives and firearms. The limitations of diffraction led to a strong interest in utilizing shorter wavelengths in order to maintain a reasonable image resolution [1]. Frequencies in the millimeter-wave (mmWave) range thus have become the favorite choice for most vendors despite the high cost burden associated. Most of security checkpoints today still rely on the conventional walk-through metal detector (WTMD) gates for screening purposes. WTMD gates are only capable to detect ferrous materials, and thus are best suited for detection of firearms. Non-metal threats cannot be detected with WTMD gates, including for instance improvised explosive devices (IED), plastic and powder explosives, liquids, and even ceramic knifes. Microwave imagers, on the other hand, are sensitive to metallic and non-metallic objects irrespective of their ferrous properties. Therefore, they were primarily developed to serve the airport demands, by pushing the boundaries in RF integration. Modern advances in semiconductor industry have unlocked the possibilities to construct large scale microwave imagers and enabled the signal processing speeds essential for the subsequent image formation and analysis. The public security market, such as mass transit systems and stadiums, is more cost sensitive and yet still struggles to benefit from these recent achievements despite present security gaps [2].

In this review paper, a historical overview of the evolution of electromagnetics in enabling microwave imaging methods is presented in Section II, followed by a discussion on the underlying principles and challenges in modern microwave imaging in Section III through Section VII. Section VIII presents modern examples on security scanners followed by an outlook.

II. EVOLUTION OF IMAGING

The research on imaging systems and methods has started in the history of humanity with the investigations on the human visual system, namely the eye. It is the human most important sensing organ which can perceive light to construct images of objects at largely varying distances. Therefore, the early investigations were made in the visible spectrum, where light is easily detected by the naked eye. The interests had ranged from the foundation of mirrors to the searching for methods to assist and enhance the visual capability of the human, like magnifying optics. From a scientific point of view, the inherent operation principle of the human eye was of a major interest, as well as the nature of light itself.

The ancient Greeks in Alexandria, located on the north shore of Egypt, conducted research on the properties of light. Euclid (estimated to have lived around 300 BC) discussed his observations on the visibility of a seen object in dependence on angular width. Heron of Alexandria (lived around AD 40) suggested novel ways for the usage of planar and curved mirrors, followed a century later by the work of Ptolemy (lived around AD 140) on reflection and refraction of light. Thanks to these efforts, early understanding of the nature of light was achieved. It was, however, believed that the eye emits rays of infinite velocity and receives them back to see an image. This understanding is interestingly well-demonstrated by Heron in his "Catoptrica" [3]. While the original work was lost, fortunately the ancient text is still available through several translations.

It took, however, around a thousand years until the scientific work of Al-Hasan Ibn Al-Haytham, and often known as Alhazen, could explain the human eye to be a passive receiver. His work was published around AD 1021 in Kitab al-Manazir, which is famously known as Book of Optics [4]. His unprecedented scientific methods have led to the first explanation of the formation of images using the camera obscura [5], [6] or pinhole image, which was observed for many centuries before [7].

It took humanity another half a millennium to discover the wave nature of light, through the ingenious work of Christiaan Huygens (1629 - 1695). As he delivered the initial description of light as being a "wave," which strongly contradicted the corpuscular theory of light defended by Newton (1642 - 1727) in his documented book "Opticks" [8], an experimental validation was to confirm his theory. At the turn of the 19th century, Young has reported the long outstanding experimental proof with his famous double-slit experiment [9], through which the Newtonian assumptions for light were finally put to rest.

After many magnificent contributions from Ampere (1775 - 1836), Gauss (1777 - 1855), Faraday (1791 - 1867), and Weber (1804 - 1891), the mathematical framework for the electromagnetic waves was completed and formulated by James Clerk Maxwell (1831 - 1879), as published in his impressive work collection "Treatise on Electricity and Magnetism" published in 1873 [10]. Following Maxwell's achievement, Heinrich Hertz (1857 - 1894) could experimentally verify that the propagation of electromagnetic waves follows the same speed of light predicted by Maxwell's mathematical findings. His paper [11] has thus proven that any electromagnetic radiation may enable imaging capabilities as much as light can enable vision in the optical spectrum.

FIGURE 1. First compact digital camera invented in 1970s. The picture size was 100x100 pixels and the data was recorded on a cassette tape. (Courtesy of the George Eastman Museum with permission from Eastman Kodak Company).

During the 20th century, the remarkable advances in the electronic industry had led to fundamental changes in the imaging methods. In photography, the first invention of a digital camera was achieved in the 1970 s, Fig. 1, whereas microwave imaging was demonstrated in radiometry by the 1974 Nobel Prize laureates in Physics, namely Martin Ryle and Antony Hewish [12]. Since then, synthetic aperture methods became widely utilized in airborne and spaceborne imaging systems for applications related to remote sensing and reconnaissance.

With the 21st century evolving, imaging methods could further advance thanks to the technology progress in semiconductors [13] and signal processing techniques [14]. The last two decades have delivered unprecedented level of innovations to enable practical use of microwave and millimeter-wave imaging capabilities in applications beyond earth observation. Most known is in security domain for personnel screening. Being a technology driver, these advances have played a major role in extending microwave imaging to new arenas as well.

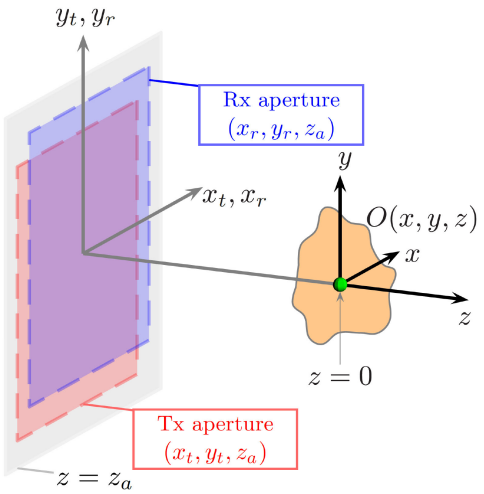

FIGURE 2. General geometrical description of planar imaging arrays. The Tx and Rx apertures are populated with antenna elements for transmitting and receiving towards the imaged object, which is centered at the coordinate origin.

III. IMAGE FORMATION

Imaging humans in the microwave and mmWave frequency ranges (3 GHz to 300 GHz) is practically possible only in reflection settings. In order to achieve a reasonable image resolution for threat detection purposes, most of the security scanning systems tend to rely on frequencies beyond 10 GHz, which would not provide any transmission imaging. In reflection imaging context, a generalized description of planar apertures can be seen in Fig. 2, in which a transmitter (Tx) and a receiver (Rx) array of antennas are present. Forming an image is achieved by focusing the signals into individual pixels. This focusing procedure can be conducted physically, i.e., by means of phased arrays or focusing lenses, or alternatively by virtual means as in the SAR methods. Conventionally, SAR systems assume a mechanical scan of the imaged scenery, as it is essential for airborne and spaceborne SAR. On the contrary, imaging in a stationary setting can be directly achieved without mechanical scanning. In that case, data collection can be performed electronically, while image formation and focusing may follow synthetically.

For the sake of simplicity and reduction of the signal processing requirements, image formation often relies on the first Born approximation [15], in which the scatters are assumed to be electrically weak and independent, resulting in a separable response of the scattered field. While this is not a valid assumption in many practical scenarios [16], e.g., metallic guns or other conductive materials, the approximation has proven applicable, nevertheless. Partially because of the fact that in security imaging one is most interested in detecting the presence of a threat. Having the first Born approximation invalidated typically contributes to an image artefact, which itself can be used to detect the presence of a concealed item [17].

Microwave imaging arrays can assume many geometries, e.g., planar, cylindrical, spherical, etc. For all imaging arrays, the image formation entails correction of the signal delays for coherent summation of the reflected scattered signals s back into a focused image. In mathematical terms, this can be stated as

$$\text{Image}(\vec{r_v}) = \sum_{\forall k}\sum_{\forall \vec{r_t}}\sum_{\forall \vec{r_r}} s(k, \vec{r_t}, \vec{r_r}) \times \exp[+jk(|\vec{r_t} - \vec{r_v}| + |\vec{r_r} - \vec{r_v}|)] \quad (1)$$

The $\vec{r_t}$ and $\vec{r_r}$ denote all vectors pointing towards any transmitter antenna at (x_t, y_t, z_a) and any receive antenna at (x_r, y_r, z_a), respectively. Whereas $\vec{r_v}$ presents a vector pointing towards the target voxel at (x, y, z) for focusing.

Equation (1) basically describes the space domain representation of the imaging process as being the coherent summation of all signal portions across all transmit-receive combinations. This coherent summation is conventionally known as the back-propagation or back-projection algorithm. In signal processing terminology, this inversion presents a matched filtering method for the phase term while ignoring the magnitude term [14], [18].

Despite the fact that (1) seems intuitive, it does not reveal much of the imaging system capabilities in terms of spatial resolution. For this purpose, the equivalency of (1) in the spatial frequency domain is preferred.

The scattering matrix s can be transformed into the Fourier domain using a four dimensional operation as

$$S(k, k_{x_r}, k_{y_r}, k_{x_t}, k_{y_t}) = \mathcal{F}_{4D}\{s(k, x_r, y_r, x_t, y_t)\} \quad (2)$$

Whereas, the spatial frequency components are geometrically related through

$$k_x = k_{x_t} + k_{x_r} \qquad k_y = k_{y_t} + k_{y_r} \quad (3)$$

$$k_z = \sqrt{k^2 - k_{x_t}^2 - k_{y_t}^2} + \sqrt{k^2 - k_{x_r}^2 - k_{y_r}^2} \quad (4)$$

By applying the Fourier transformation on both sides of (1) along with the method of stationary phase [19], one can drive the image inversion equation [17] to be

$$\text{Image}(\vec{r_v}) = \mathcal{F}_{3D}^{-1}\{\mathcal{F}_{4D}\{s\} \times \exp(-jk_z z_a)\} \quad (5)$$

Equation (5) introduces the spatial frequency domain representation of the image inversion process defined in (1). The equation reveals that the image formation can be conducted through a Fourier transformation of the scattering function s, followed by a phase correction term based on the focusing range, and concluding by an inverse Fourier transformation in order to gain the full 3D image. While this inversion seems simple to implement at first glance, the numerical implementation of the inversion often entails complex nonlinear interpolations [14], [20]–[22]. When imaging at short ranges, even an equidistant sampled aperture will cause the function S to become irregularly sampled due to the nonlinear relation in (4). A dedicated numerical implementation is therefore always needed to match the specific system aperture design and sampling scheme.

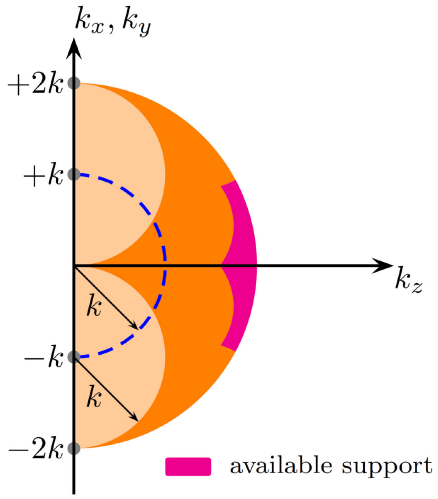

FIGURE 3. The allocation of *K*-space for a square multistatic array operating with a single frequency and imaging a point target at distance *L* equal to its aperture width *D*.

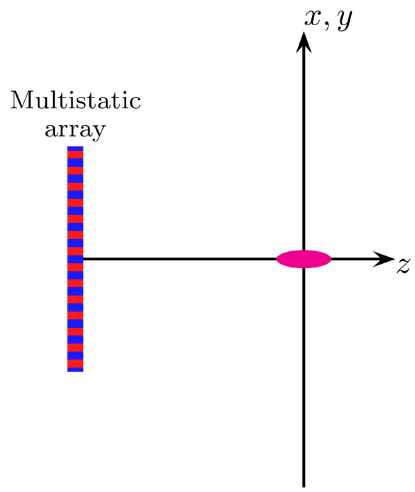

FIGURE 4. The corresponding shape of the focused spot present at distance *L*. The resolution at this location directly relates to the allocation of the *K*-space highlighted in Fig. 3.

IV. IMAGE RESOLUTION

The spatial resolution of an imaging system is best driven by the available signal allocation in the spatial frequency domain, namely the distribution of (k_x, k_y, k_z), often also known as the signal support within the K-space. The framework described by (5) is generalized enough to help determine the maximum achievable support for any planar array geometry and at all focusing distances. In security screening, systems tend to operate at short ranges, causing the K-space to undertake an extended allocation. This is advantageous in enhancing the imaging resolution, however comes at the cost of higher computation requirements due to the increase of non-linearity according to (4).

The K-space allocation for planar multistatic arrays can be sketched as in Fig. 3. The maximum allocation can stretch to a hemisphere of $2k$ radius. For the practical case of finite imaging arrays, the signal support concentrates at the far right highlighted portion. Fig. 4 illustrates the corresponding array geometry and focusing spot to the signal support in Fig. 3.

Monostatic arrays are a special case of multistatic arrays in which the signal reception is restricted to be at the same transmitter location. Monostatic data acquisition is widely used in satellite SAR for instance. Their signal support in K-space will accordingly assume a thinner shell of the highlighted area of Fig. 3.

The formulation of the spatial resolutions of a general planar array can now be driven. Assuming a square-shaped array of an aperture width $D_{\blacksquare}$ and a general distribution of transmitter and receiver arrays, i.e., multistatic case, the Cartesian cross-range resolution is given by

$$\delta_{x,y} = \frac{c_0}{4f^{\max}} \times \sqrt{4\,(L/D_{\blacksquare})^2 + 1} \tag{6}$$

whereas c_0 and $f^{\max}$ denote the speed of light and the maximum operating imaging frequency, respectively. The focusing range is indicated by L. The ratio $(L/D_{\blacksquare})$ determines the enhancement in cross-range resolution due to the angular diversity present in the short-range imaging. Similarly, the range resolution can be calculated to be

$$\delta_z = \frac{c_0/2}{\Delta f + \left(1 - \frac{1}{\sqrt{1+\frac{1}{2}(D_{\blacksquare}/L)^2}}\right) \times f^{min}} \tag{7}$$

In which the Δf and f^{min} denote the total signal bandwidth and the minimum operating imaging frequency. Noticeably, the range resolution does not only depend on the signal bandwidth, but also on the absolute operating frequency. On the contrary to the long range radar systems, short range imaging can deliver better range resolution when operates at higher frequencies, e.g., mmWaves and THz band. Additionally, monofrequent systems can still offer range resolution even for zero Δf, a phenomenon similar to the depth of field terminology known in photography.

When imaging systems transition from short range to long range operation, the ratio $(L/D_{\blacksquare})$ becomes much greater than unity. The resolution equations above thus asymptotically converge to the far-field formulations

$$\delta_{x,y}^{\text{far-field}} = \frac{c_0}{2f^{\max}} \times \left(\frac{L}{D_{\blacksquare}}\right) \tag{8}$$

$$\delta_z^{\text{far-field}} = \frac{c_0}{2\Delta f} \tag{9}$$

V. IMAGING ARRAYS

Out of all possibilities to build imaging arrays, multistatic ones are considered state-of-the-art in image quality and performance. Multistatic arrays do not restrict the sampling of the receive signal to be co-located to the transmitter. Therefore, they are considered to be a generic form of the imaging arrays and hence are presented here in greater detail. It is worth mentioning that monostatic arrays in particular are extensively deployed in satellite and airborne SAR systems due to the natural flight constraints engaged. In a two-dimensional array, such mechanical constraints are no more imposed and instead an antenna array can be realized to coherently transmit and receive at multiple different locations. As seen next, multistatic arrays can help reduce the number of antenna elements and avoid the regular dense aperture sampling required by monostatic arrays.

Multistatic arrays were introduced and deployed earlier in ultrasonic imaging [23]. Efforts for establishing a mathematical equivalency to monostatic arrays were often intended in order to enable the utilization of available SAR algorithms. However this is not always applicable for short range microwave imaging, those mathematical representations can still offer guidance to understand the characteristics of multistatic imaging arrays. The Following formulation presents the basic relationships between the Tx and Rx sub-arrays in a multistatic system

$$\begin{aligned} \mathrm{AF} &= \mathrm{AF}_{\mathrm{Tx}} \cdot \mathrm{AF}_{\mathrm{Rx}} \\ &= \mathcal{F}_{2D}\{a_{\mathrm{Tx}}\} \cdot \mathcal{F}_{2D}\{a_{\mathrm{Rx}}\} \\ &= \mathcal{F}_{2D}\{\underbrace{a_{\mathrm{Tx}} * a_{\mathrm{Rx}}}_{a_{\mathrm{Eff}}}\} \end{aligned} \tag{10}$$

The $\mathrm{AF}_{\mathrm{Tx}}$ and $\mathrm{AF}_{\mathrm{Rx}}$ denote the array factors of the transmit and receive sub-arrays, respectively. Considering that the array factor is driven by the Fourier transformation of the array geometry, the overall array factor of the transmit-receive array is given by the convolution outcome of both sub-arrays. An effective Tx-Rx array can thus be defined as a_{Eff}, which is often also called the virtual aperture. The convolution process allows for different possibilities in realizing the individual Tx and Rx sub-arrays, in which the convolution outcome is still identical. Fig. 5 presents examples of equivalent multistatic arrays, while the individual Tx and Rx sub-arrays assume varying geometries.

Multistatic arrays when realized in 1D or 2D arrangement can deliver 2D and 3D images, respectively. As the array performance relates to the convolution outcome of the Tx and Rx apertures, the actual physical array entails significantly less resources compared to the equivalent monostatic case. For instance, if N_T transmitters and N_R receivers are deployed, a total of virtual $N_T \times N_R$ elements are achieved with only $N_T + N_R$ actual channels. This reduction can be massive for large scale arrays. Consequently, mmWave arrays constructing millions of virtual elements may be constructed by deploying only a few thousand elements. It is worth mentioning that multistatic arrangements of minimal resources can only be achieved with redundancy-free allocation, e.g., no repetitions in the virtual element locations. In reality, redundancy-free is barely possible at large scale arrays. Nevertheless, the reduction in resources typically outscores the redundancy factors engaged.

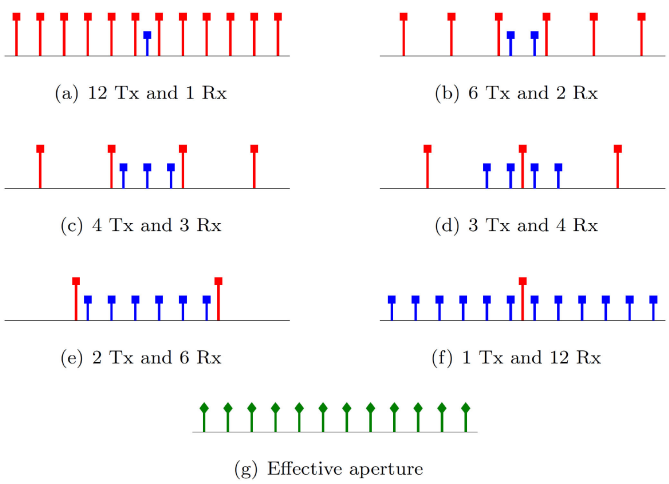

FIGURE 5. Different arrangements for multistatic arrays yielding the same effective aperture.

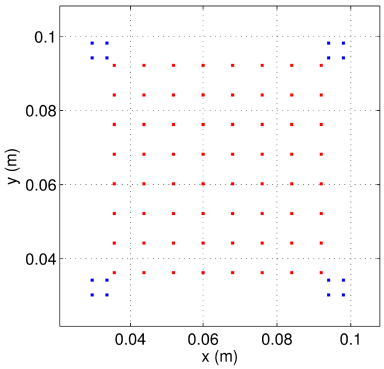

FIGURE 6. Example of 2D multistatic array arrangement. Inner red dots denote transmitters (Tx) and outer blue dots receivers (Rx) locations.

For security screening, imaging at short distances is vital. The multistatic effective arrays hold strictly true only at far ranges, therefore the design of short range operation is subject to numerical optimizations in order to balance the image quality with the level of redundancy allowed. Successful deployment of multistatic imaging arrays at short distances has been reported in literature as in [24]. Fig. 6 presents an example 2D multistatic array tile. Using 4x4 arrangement of that array tile, the focusing performance as in Fig. 7 a and 7 b can be achieved. The individual point spread functions (PSFs) detail the focusing pattern and possible artefacts. The collective focusing quality of the Tx-Rx array, i.e., full multistatic operation, is calculated by the spatial multiplications of the two PSFs, yielding the result in Fig. 8.

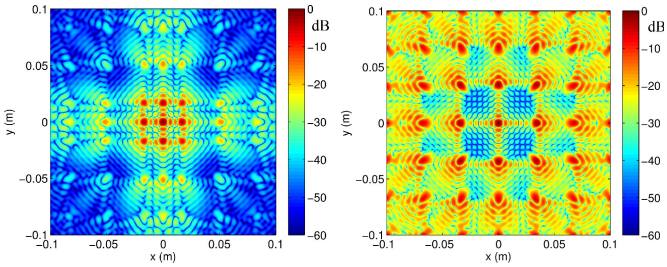

(a) PSF of Tx sub-array (b) PSF of Rx sub-array

FIGURE 7. Individual focusing patterns of the sub-arrays.

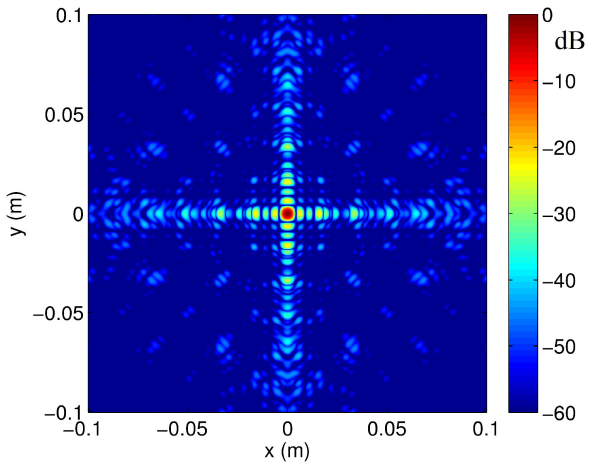

FIGURE 8. Two-way PSF after focusing the Tx and Rx of a 4x4 array arrangement shown in Fig. 6.

VI. IMAGING PERFORMANCE

In the endeavor of establishing new imaging methods with innovative scanning modes, the lack of standards or definitions for image quality makes it difficult to keep track of the enhancements in imaging performance. Often experts would still rely on subjective means to judge the image quality, which could be misleading. While in the design phase, most of the image quality indications are evaluated using the PSF, in practice other effects become also relevant.

In security scanners, the challenge of full characterization of image quality becomes even harder due to the strong varying nature of the measured subject, more specifically, the human body. Accordingly, in the recent years, subject matter experts have commenced to establish a dedicated standard for mmWave security imaging systems, namely the ANSI 42.59 under the tentative title "Imaging Performance of Active Millimeter-Wave Systems for Security Screening of Humans". The standard addresses the security screening for airport checkpoints. While the standard is still under development, the list in Table 1 summarizes the major selected quality metrics therein. It is worth noting that other metrics are expected to be included in future releases, like motion blur, phase stability, etc.

TABLE 1. Overview of the Current Image Quality Metrics Considered in the Forthcoming ANSI 42.59 Standard

Quality Metric	Description
Lateral Resolution	Separability between finite objects or edges parallel to the aperture
Depth Resolution	Separability between object layers perpendicular to the aperture
Illumination Coverage	Extent of observable illumination on a smooth target within the imaging space
Dynamic Range	Measure of the least distinguishable object in the image, e.g., metallic spheres
Contrast Resolution	Measure of the linearity of the image at different reflectivity levels

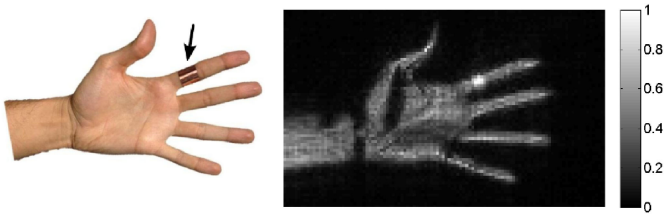

FIGURE 9. Comparing human skin reflection relative to metals in the mmWave range. Due to the dominant water content of the skin, the reflection coefficient is about 60%.

VII. IMAGING HUMANS

Screening of humans with microwaves is particularly challenging. The highly varying nature of the human body contours often leads to shadowing effects and illumination limitations. In order to understand this problem, one should look into the electrical properties of human skin across the microwave spectrum [25]–[27]. Human skin has relatively high permittivity due to the dominant water content, which consequently leads to an impedance mismatch when illuminated by an RF signal. In addition, human skin is electrically smooth for wavelengths down to a millimeter or less, and hence also accounts for strong specular reflections. Consequently, security scanners need to be designed to mitigate these challenges in order to maintain sufficient threat visibility. Otherwise, the threat detection might get easily compromised by the complex contours of the human body. Fig. 9 illustrates a practical example for the visibility of human skin when applying active illumination.

The specular reflection on the skin at mmWaves suggests the simulation of skin response using adapted physical optics (PO) algorithms [17]. In Fig. 10 and Fig. 11, a simulation for a full sized active body scanner is presented. The illumination results reveal the body zones which can be captured by the imaging array probably. In order to maximize the illumination coverage around the body, vendors rely on well-define stance, ambient and diverse illumination, motion aggregation, and other techniques.

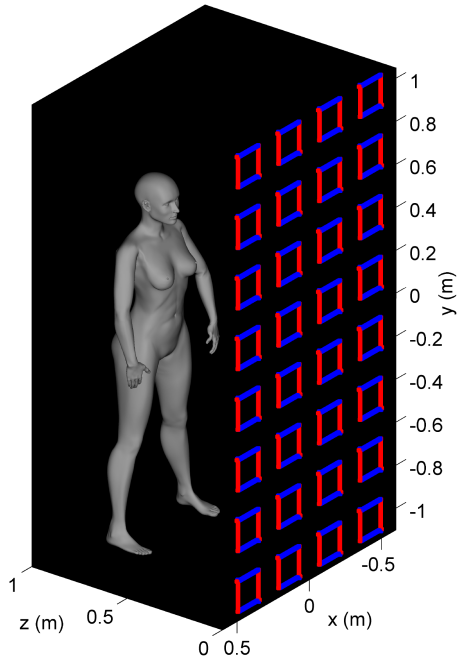

FIGURE 10. Geometry illustration for a simulation scenario of a full female body while imaged with one meter wide and 2 meter height scanner.

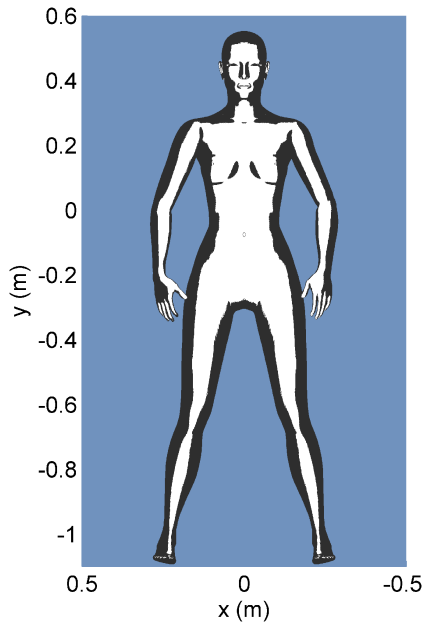

FIGURE 11. Simulation result for the geometry in Fig. 10. The white areas denote the visible skin portions, whereas the dark gray are invisible zones due the specular reflections.

VIII. SECURITY SCANNERS

The last two decades have witnessed several successful demonstrations of full body scanning systems in the microwave and mmWave ranges. Diverse scanning methods have been implemented, ranging from mechanical to fully electronic, and from passive to active operation. Most of these scanners have been developed to serve the security applications, either in a checkpoint environment or in an uncontrolled security setting. While airports are a prominent example of a checkpoint security, public security applications such as mass transit systems, stadiums, and shopping malls have also gained a lot of attention recently.

In the following sections, a discussion on these full sized systems is presented. The purpose is to showcase the major innovations achieved in the past two decades and is surely not meant to compile a full list of successful demonstrations. Readers are encouraged to review the cited publications and the other resources therein.

A. PASSIVE SYSTEMS

Passive image formation relies primarily on radiometric techniques for the receiving and focusing of the radiation field out of the human body [28]. The received energy in this case is composed of a combination of the thermal radiation and the skin reflections from ambient illumination. The former is governed dominantly by the surface temperature, therefore a detection of a concealed threat would require it to assume a different temperature rather than the background skin. Metal threats, e.g., guns, are accordingly easier to recognize compared to dielectric explosive threats.

Passive imaging is particularly favorable for stand-off detection. When imaging at a far distance, active systems suffer signal losses and sever limitations form specular reflections. Considering that passive systems inherently produce a factor of two coarser lateral resolution due to the one-way signal propagation, it is often desired to operate the scanners at higher frequency ranges. While higher frequencies could restore the resolution, they are subject to extensive propagation losses and cloth penetration limitations as well.

For outdoor scenarios, the detection can rely more on ambient illumination from the surroundings including the sky and the sun. An early success on passive imaging in outdoor settings was reported in [29]. For instance, an exemplary image at 94 GHz is shown in Fig. 12. It also illustrates the strong skin reflection of the sky background illumination due the specular reflection effects, most noticeable around the shoulders, the upper head, and the knife blade.

In the last two decades, more advances in passive detection and imaging have been reported [30]–[32]. Detection sensitivities in sub-kelvin range have been proven realizable by several research groups [33]–[38]. And a couple have been commercialized based on either cooled or uncooled receivers. An image is presented in Fig. 13, which was acquired at 5 meter distance with an ARGON scanner [39], [40]. The image reveals a concealed rifle on a human body.

B. ACTIVE SYSTEMS

Most of the widely deployed commercial systems for security checkpoint entail active operation. Active imaging can maintain an adequate level of robustness against environmental conditions and does not rely on external sources like sky illumination. Active imagers can also operate at mmWave

FIGURE 12. Outdoor passive image at 94 GHz using sky background illumination. (Copyright© 2007 IEEE. Reprinted, with permission, from [29]).

FIGURE 13. Indoor passive image utilizing thermal radiation from 200 GHz to 600 GHz. Taken from 5 meters distance. (Reproduced with permission from Company Asqella Oy).

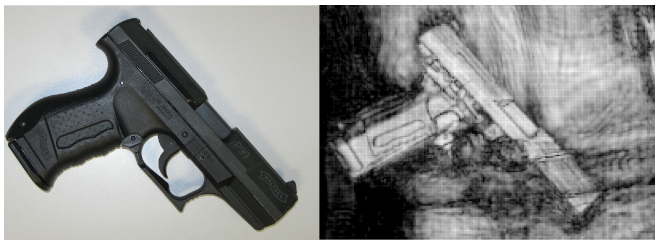

(a) Picture (b) Concealed gun in mmWaves

FIGURE 14. Example of the level of details which can be achieved in the mmWave range [17]. The gun was concealed behind a thick pullover and a leather belt.

(a) mm-wave image (b) optical image

(a) Plastic PETN sample packed in a thin plastic bag on a metal background.

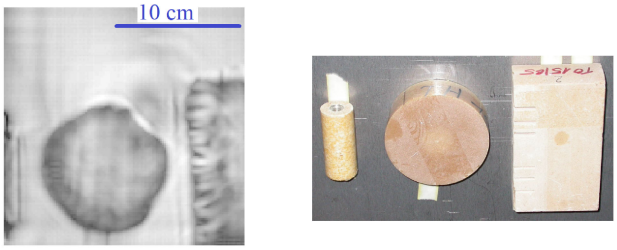

(a) mm-wave image (b) optical image

(b) Variations of TNT mounted with double sided tape on a metal background.

FIGURE 15. Exemplary mmWave images of explosive substances at 75 GHz on 30 dB scale. (Copyright© 2009 IEEE. Reprinted, with permission, from [41]).

ranges without being constrained by the thermal radiation of the imaged subjects. Additionally, high resolution with wide dynamic range is easier to achieve in active operation and to be adjusted by design. This allows a great benefit in balancing the required cloth penetration with the image quality metrics. As discussed next, most of the commercial systems operate between 10 and 100 GHz, or equivalently 30 to 3 millimeter in wavelength. Fig. 14 presents an example of an active image acquired around the 4 mm wavelength for a gun while being concealed behind a thick pullover and a leather belt.

Threat detection in security screening is no more limited to metallic targets, like the gun in Fig. 14, however is concerned by the detection of explosive substances either in bulk or when constructed as an IED. Therefore, it is essential for the detection algorithms to distinguish the response of these materials in the microwave range. Fig. 15 displays mmWave image examples of TNT variants as well as a packed plastic PETN sample. Interestingly, most of the chemical compounds used in explosive threats pose low to moderate attenuation for the microwave signals, hence making them feasible to locate and recognize in mmWave images [41].

The last two decades have delivered remarkable advances in innovative solutions for realizing full scale active imaging capabilities. These efforts started off with the published work of the Pacific Northwest National Laboratory (PNNL) [42]. The technology is based on a combined mechanical scan and an electronic vertical monostatic array for full scale body imaging. The mechanical scan can be performed cylindrically for enhanced illumination. The technology is currently commercialized by Company Leidos under the model name ProVision.

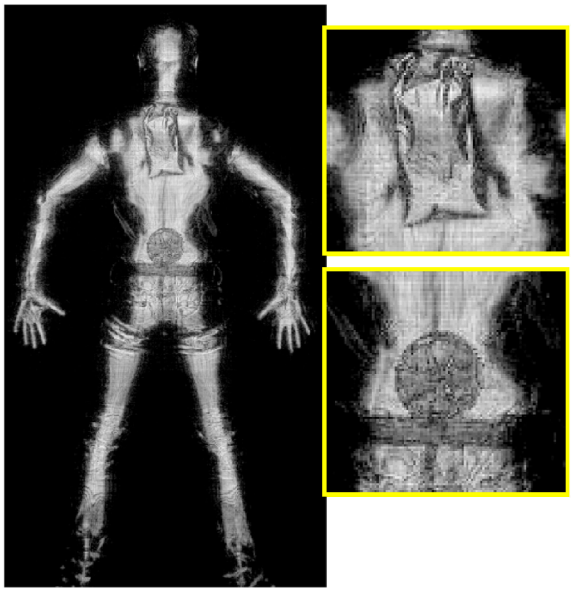

FIGURE 16. Active image in the 70 GHz to 80 GHz frequency band. The imaged person is concealing surrogates of a liquid and plastic explosives [17].

A few years later, a fully electronic solution was published by Agilent Technologies as in [43]. The scanning is based on a Fresnel lens in reflection configuration. Individual antenna elements were adjusted for mono-frequency operation at 24 GHz while being controlled electronically to steer the focal spot. For full body screening, the passenger would be required to rotate in front of the panel. This solution was also commercialized later by the Company Smiths Detection under model name eqo™.

Early in the last decade, first fully electronic mmWave imagers were invented as in [44]–[46]. The technology utilized dedicated multistatic imaging transceivers in flat panel topology in order to enable high fidelity imaging in the 70 to 80 GHz frequency band. An image example is presented in Fig. 16. In dual panel configuration, the scanner is able to deliver full body screening. This solution has also been commercialized by the Company Rohde&Schwarz under the model name R&S®QPS.

Airport security is regulated by national and international security agencies, e.g., the European Civil Aviation Conference (ECAC) in Europe and the Transportation Security Administration (TSA) in the US. Security agencies define the level of performance required for certifying the equipment prior to their deployment at the airport. For instance, ECAC regularly publishes a list of vendors and scanner models, which were able to pass the detection performance evaluation. In ECAC terminology, the detection can be either automatic (Type A) or manual (Type B). Type A security scanner shall be capable to provide automatic threat detection with indication of the location of detected objects on an anonymous figure or avatar, whereas Type B security scanner relies on a human reviewer to analyze the image.

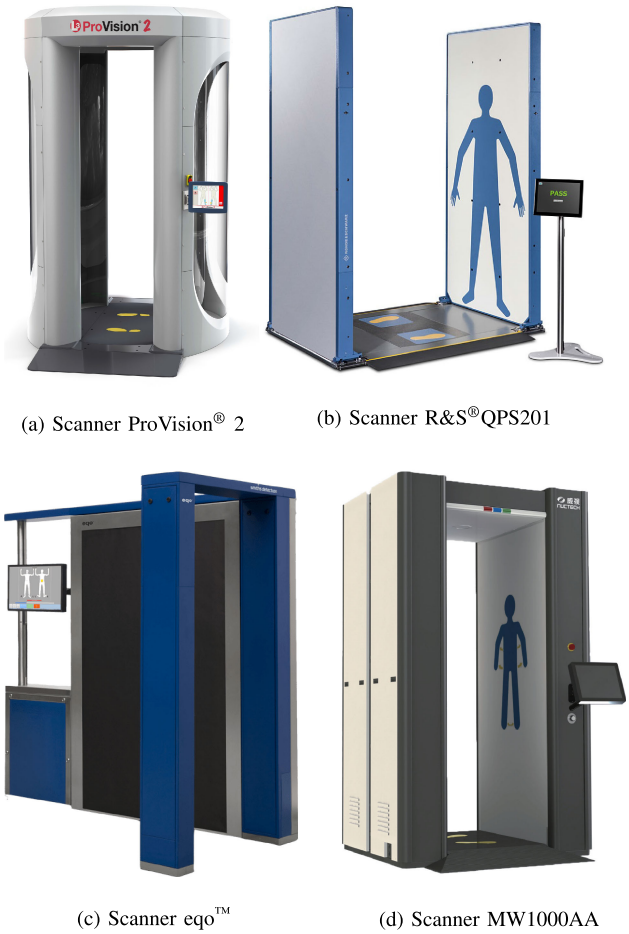

(a) Scanner ProVision® 2 (b) Scanner R&S®QPS201

(c) Scanner eqo™ (d) Scanner MW1000AA

FIGURE 17. Photograph of commercialized body scanner products listed in Table 2.

Table 2 summarizes the currently published ECAC list of Type A security scanners of the highest detection standard. The corresponding imaging operation methods are indicated according to the vendors' publications. Fig. 17 presents photographs of the scanner systems.

IX. OUTLOOK

The last two decades have fundamentally changed the perception of microwave imaging capabilities towards becoming affordable and deployable in daily use. Security screening has benefited most from these advances, while the public shows currently more acceptance than ever to the technology, especially when paired with machine detection functionality to prevent any privacy infringing concerns. Despite this success, the journey for microwave imaging is still at the start. Researchers around the globe are continuously reporting enhancements on the array design, hardware implementation, image formation, and image interpretation. Early successes for imaging beyond first Born approximation are evolving as well, which may enable material classification as well as imaging inside enclosures like shoes [55] and thick clothing. The rapid increase in the computation power also provides the

TABLE 2. Commercial Systems Currently Certified by ECAC [47] for Automatic Threat Detection With Standard 2 Capability. The List is a Snapshot of Currently Available Solutions and is Not Meant to be a Complete List of all Commercial Vendors

Provider	Model	Frequency Range	Waveform	Scan Mode
Leidos [48], [49]	ProVision® 2	24-30 GHz	FMCW	Hybrid electronic and mechanical
Rohde&Schwarz [50]	R&S®QPS201	70-80 GHz	SFCW	Fully electronic
Smiths Detection [51]	eqo™	24 GHz	CW	Fully electronic with passenger rotation
Nuctech [52]–[54]	MW1000AA	32-38 GHz	SFCW	Hybrid electronic and mechanical

resources to utilize sophisticated signal processing schemes and to further increase the array sparseness for cost reduction [56]–[59]. The III-V semiconductors, e.g., SiGe, as well as CMOS integrated solutions became capable to provide hybrid digital and analog integration for mmWave transceivers, making the design of large scale imaging arrays within reach.

With the cost of semiconductors and their integration dropping steadily, the new decade is expected to showcase the first mmWave real-time imaging capability in order to achieve a convenient walk-through scanning procedure, and hopefully to enable affordable microwave security imaging to serve at public spaces as well.

REFERENCES

[1] R. Appleby, D. A. Robertson, and D. Wikner, "Millimeter wave imaging: A historical review," in *Proc. SPIE Passive Act. Millimeter-Wave Imaging Conf. XX*, 2017, vol. 10189, pp. 1–13. [Online]. Available: https://doi.org/10.1117/12.2262476

[2] "Mass attacks in public spaces," Aug. 2020. [Online]. Available: https://www.secretservice.gov/data/protection/ntac/MAPS2019.pdf

[3] M. R. Cohen and I. E. Drabkin, *A Source Book in Greek Science*. Cambridge, MA, USA: Harvard Univ. Press, 1948.

[4] A.-H. Ibn Al-Haytham (Alhazen), *Book of Optics (Kitab Al-Manazer)*, 1021.

[5] D. C. Lindberg, "Alhazen's theory of vision and its reception in the west," *Isis*, vol. 58, no. 3, pp. 321–341, 1967.

[6] D. C. Lindberg, "The theory of pinhole images from antiquity to the thirteenth century," *Arch. Hist. Exact Sci.*, vol. 5, no. 2, pp. 154–176, 1968.

[7] D. Diderot and J. le Rond d' Alembert, *Encyclopédie, ou Dictionnaire Raisonné des Sciences, des Arts et des Métiers*, par une Société de Gens de lettres, 1772.

[8] T. Newton, *Opticks or a Treatise of the Reflections, Refractions, Infections and Colours of Light*. London, U.K.: Printed for Sam Smith and Benj Walford, 1704.

[9] T. Young, "An account of some cases of the production of colours, not hitherto described," *Philos. Trans. Roy. Soc. Lond.*, vol. 92, pp. 387–397, 1802.

[10] J. C. Maxwell, *Treatise on Electricity and Magnetism*. Oxford, U.K.: Clarendon, 1873.

[11] H. Hertz, "Ueber die Ausbreitungsgeschwindigkeit der electrodynamischen Wirkungen," *Annalen der Physik und Chemie*, vol. 270, no. 7, pp. 551–569, 1888.

[12] Ryle, and Martin, "Radio Telescopes of Large Resolving Power," *Nobel Lecture*, Jun. 1974.

[13] P. Hillger, J. Grzyb, R. Jain, and U. R. Pfeiffer, "Terahertz imaging and sensing applications with silicon-based technologies," *IEEE Trans. THz Sci. Technol.*, vol. 9, no. 1, pp. 1–19, Jan. 2019.

[14] M. Soumekh, *Fourier Array Imaging*. Upper Saddle River, NJ, USA: Prentice-Hall/PTR, 1994.

[15] M. Born and E. Wolf, *Principles of Optics*. New York, NY, USA: Pergamon, 1980.

[16] S. S. Ahmed and L. Schmidt, "Illumination of humans in active millimeter-wave multistatic imaging," in *Proc. 6th Eur. Conf. Antennas Propag.*, 2012, pp. 1755–1757.

[17] S. S. Ahmed, *Electronic Microwave Imaging with Planar Multistatic Arrays*. Berlin, Germany: Logos Verlag, 2014.

[18] E. Wolf, "Three-dimensional structure determination of semi-transparent objects from holographic data," *Opt. Commun.*, vol. 1, no. 4, pp. 153–156, 1969.

[19] A. Papoulis, *Systems and Transforms With Applications in Optics*. New York, NY, USA: McGraw-Hill, 1968.

[20] R. H. Stolt, "Migration by Fourier transform," *Geophysics*, vol. 43, no. 1, pp. 23–48, 1978.

[21] M. Soumekh, "Bistatic synthetic aperture radar inversion with application in dynamic object imaging," *IEEE Trans. Signal Process.*, vol. 39, no. 9, pp. 2044–2055, Sep. 1991.

[22] M. Soumekh, "A system model and inversion for synthetic aperture radar imaging," *IEEE Trans. Image Process.*, vol. 1, no. 1, pp. 64–76, Jan. 1992.

[23] G. R. Lockwood and S. F. Foster, "Optimizing sparse two-dimensional transducer arrays using an effective aperture approach," in *Proc. Ultrason. Symp.*, 1994, pp. 1497–1502.

[24] S. S. Ahmed, A. Schiessl, and L.-P. Schmidt, "Near field mm-Wave imaging with multistatic sparse 2D-arrays," in *Proc. 6th Eur. Radar Conf.*, 2009, pp. 180–183.

[25] T. Wu, T. S. Rappaport, and C. M. Collins, "The human body and millimeter-wave wireless communication systems: Interactions and implications," in *Proc. IEEE Int. Conf. Commun.*, 2015, pp. 2423–2429.

[26] F. Gustrau and A. Bahr, "W-band investigation of material parameters, SAR distribution, and thermal response in human tissue," *IEEE Trans. Microw. Theory Techn.*, vol. 50, no. 10, pp. 2393–2400, Oct. 2002.

[27] C. Gabriel, S. Gabriel, and E. Corthout, "The dielectric properties of biological tissues: I. Literature survey," *Phys. Med. Biol.*, vol. 41, no. 11, pp. 2231–2249, Nov. 1996.

[28] N. A. Salmon, "Indoor full-body security screening: Radiometric microwave imaging phenomenology and polarimetric scene simulation," *IEEE Access*, vol. 8, pp. 144 621–144 637, 2020.

[29] R. Appleby and H. B. Wallace, "Standoff detection of weapons and contraband in the 100 GHz to 1 THz region," *IEEE Trans. Antennas Propag.*, vol. 55, no. 11, pp. 2944–2956, Nov. 2007.

[30] H. Feng *et al.*, "A passive video-rate terahertz human body imager with real-time calibration for security applications," *Appl. Phys. B*, vol. 126, no. 8, Aug. 2020, Art. no. 143.

[31] M. Kowalski, "Hidden object detection and recognition in passive terahertz and mid-wavelength infrared," *J. Infrared Millimeter THz Waves*, vol. 40, pp. 1074–1091, 2019.

[32] R. Li, C. Li, H. Li, S. Wu, and G. Fang, "Study of automatic detection of concealed targets in passive terahertz images for intelligent security screening," *IEEE Trans. THz Sci. Technol.*, vol. 9, no. 2, pp. 165–176, Mar. 2019.

[33] M. Aoki, S. R. Tripathi, M. Takeda, and N. Hiromoto, "Passive imaging using a 4k-cryocooled thz photoconductive detector system with background-limited performance," in *Proc. Int. Conf. Infrared Millimeter THz Waves*, 2011, pp. 1–2.

[34] E. Heinz *et al.* "Toward high-sensitivity and high-resolution submillimeter-wave video imaging," *Opt. Eng.*, vol. 50, no. 11, pp. 1–9, 2011.

[35] E. N. Grossman, K. Leong, X. B. Mei, and W. R. Deal, "Passive 670 GHz imaging with uncooled low-noise HEMT amplifiers coupled to zero-bias diodes," in *Proc. SPIE Passive Act. Millimeter-Wave Imaging Conf. XVII*, 2014, vol. 9078, pp. 70–78. [Online]. Available: https://doi.org/10.1117/12.2050738

[36] A. Luukanen, A. J. Miller, and E. N. Grossman, "Active millimeter-wave video rate imaging with a staring 120-element microbolometer array," in *Proc. SPIE Radar Sensor Technol. VIII Passive Millimeter-Wave Imag. Technol. VII*, vol. 5410, 2004, pp. 195–201.

[37] E. N. Grossman, A. Luukanen, and A. J. Miller, "Terahertz active direct detection imagers," in *Proc. SPIE THz Military Security Appl. Conf. II*, vol. 5411, 2004, pp. 68–77.
[38] D. Becker *et al.*, "High-resolution passive video-rate imaging at 350 GHz," in *Proc. SPIE Passive Millimeter-Wave Imaging Technol. Conf. XIV*, 2011, pp. 42–50.
[39] Asqelle Oy, ARGON Scanner, Oct. 2020. [Online]. Available: https://asqella.com/argon/
[40] E. N. Grossman, C. R. Dietlein, M. Leivo, A. Rautiainen, and A. Luukanen, "A passive, real-time, terahertz camera for security screening, using superconducting microbolometers," in *IEEE MTT-S Int. Microw. Symp. Dig.*, 2009, pp. 1453–1456.
[41] A. Schiessl and S. S. Ahmed, "W-band imaging of explosive substances," in *Proc. Eur. Microw. Conf.*, 2009, pp. 1888–1891.
[42] D. M. Sheen, D. L. McMakin, and T. E. Hall, "Three-dimensional millimeter-wave imaging for concealed weapon detection," *IEEE Trans. Microw. Theory Techn.*, vol. 49, no. 9, pp. 1581–1592, Sep. 2001.
[43] P. A. Corredoura, Z. A. Baharav, B. A. Taber, and G. A. Lee, "Millimeter-wave imaging system for personnel screening: Scanning 107 points a second and using no moving parts," in *Proc. SPIE Passive Millimeter-Wave Imag. Technol. Conf. IX*, vol. 6211, 2006, pp. 62110B-1–62110B-8.
[44] S. S. Ahmed, A. Schiessl, and L.-P. Schmidt, "Novel fully electronic active real-time millimeter-wave imaging system based on a planar multistatic sparse array," in *Proc. IEEE Int. Microw. Symp.*, 2011, pp. 1–4.
[45] S. S. Ahmed, A. Schiessl, F. Gumbmann, M. Tiebout, S. Methfessel, and L. Schmidt, "Advanced microwave imaging," *IEEE Microw. Mag.*, vol. 13, no. 6, pp. 26–43, Sep./Oct. 2012.
[46] S. S. Ahmed, "Advanced fully-electronic personnel security screening technology," in *Proc. 9th Eur. Conf. Antennas Propag.*, 2015, pp. 1–4.
[47] ECAC CEP, Security Scanners SSc, Feb. 2020. [Online]. Available: https://www.ecac-ceac.org/documents/10189/62763/ECAC-CEP-SSc-Web-Update-26Feb2020.pdf
[48] Leidos, ProVision 2 Brochure, Oct. 2020. [Online]. Available: https://www.leidos.com/markets/aviation/security-detection/aviation-checkpoint/people-screening
[49] SafeView, Inc., "Request for Waiver of Sections 15.31 and 15.35 of the Commission's Rules to Permit the Deployment of Security Screening Portal Devices that Operate in the 24.25-30 GHz Range," Order, 21 FCC Rcd. 8814, ET Docket No. 04-373 (2006), Jan. 2010. [Online]. Available: https://www.fcc.gov/document/request-waiver-sections-1531-and-1535-commissions-rules
[50] Rohde & Schwarz, QPS201 Brochure, Oct. 2020. [Online]. Available: https://www.rohde-schwarz.com/us/brochure-datasheet/qps
[51] Smiths Detection, Eqo Brochure, Oct. 2020. [Online]. Available: https://www.smithsdetection.com/products/eqo
[52] Nuctech, MW1000AA Brochure, Oct. 2020. [Online]. Available: https://www.nuctech.com
[53] L. Qiao, Y. Wang, Z. Zhao, and Z. Chen, "Exact reconstruction for near-field three-dimensional planar millimeter-wave holographic imaging," *J. Infrared Millimeter THz Waves*, vol. 36, no. 12, pp. 1221–1236, Dec. 2015.
[54] L. Qiao, Y. Wang, Z. Shen, Z. Zhao, and Z. Chen, "Compressive sensing for direct millimeter-wave holographic imaging," *Appl. Opt.*, vol. 54, no. 11, pp. 3280–3289, Apr. 2015.
[55] D. M. Sheen, R. T. Clark, J. R. Tedeschi, J. McCall, T. S. Hartman, and A. M. Jones, "Efficient image reconstruction method for a millimeter-wave shoe scanner," in *Proc. SPIE Passive Act. Millimeter-Wave Imaging Conf. XXIII*, 2020, vol. 11411, pp. 34–45.
[56] T. Fromenteze, O. Yurduseven, F. Berland, C. Decroze, D. R. Smith, and A. G. Yarovoy, "A transverse spectrum deconvolution technique for MIMO short-range fourier imaging," *IEEE Trans. Geosci. Remote Sens.*, vol. 57, no. 9, pp. 6311–6324, Sep. 2019.
[57] K. Tan and X. Chen, "Fast 3-D image reconstruction on nonregular UWB sparse MIMO planar array using scaling techniques," *IEEE Trans. Microw. Theory Techn.*, early access, Sep. 4, 2020, doi: 10.1109/TMTT.2020.3019099.
[58] J. N. Gollub *et al.*, "Large metasurface aperture for millimeter wave computational imaging at the human-scale," *Sci. Rep.*, vol. 7, no. 1, Feb. 2017, Art. no. 42650.
[59] B. Gonzalez-Valdes *et al.*"Millimeter wave imaging architecture for on-the-move whole body imaging," *IEEE Trans. Antennas Propag.*, vol. 64, no. 6, pp. 2328–2338, Jun. 2016.

SHERIF S. AHMED (Senior Member, IEEE) received his M.Sc. degree in Microwave Engineering from The Technical University of Munich, Munich, Germany, in 2007, and the Ph.D. (Dr.-Ing.) degree from The University of Erlangen-Nuremberg, Erlangen, Germany, in 2013. He is currently an Adjunct Professor at Stanford University, CA, and possesses more than 15 years of professional industry experience in various research and development roles. He has coauthored more the 25 research papers, more than 20 patents, and a book on advanced microwave imaging methods. He was the recipient of the University Academic Award of the Technical University of Munich (TUM) in 2007, the Innovation Award of Rohde & Schwarz (R&S) in 2009 and 2018, and the IEEE MTT Microwave Prize Award of 2013. Moreover, he is a Co-Chair on the US ANSI standard committee for Measuring the Imaging Performance of mmWave Systems for Security Screening of Humans.

His research and development focus extends to microwave and mmWave imaging, stand-off THz sensing, multistatic radars, advanced signal-processing techniques, terahertz technology, and last but not least, automotive radar design and characterization. Over the past decade, he pioneered the body scanner technology with the first fully-electronic multistatic mmWave imaging systems, which are being deployed worldwide today at airport checkpoints. In the recent years, he has been advancing the qualifications of automotive radars, towards autonomous driving capabilities.